Ballistic Diffusion in Poly-Aromatic Hydrocarbons on Graphite

Irene Calvo-Almazán,[*,†] Marco Sacchi,[‡] Anton Tamtögl,[†] Emanuel Bahn,[¶] Marek M. Koza,[¶] Salvador Miret-Artés,[§] and Peter Fouquet[¶]

†*Cavendish Laboratory, University of Cambridge, J. J. Thomson Avenue, CB3 0HE, Cambridge, United Kingdom.*

‡*Department of Chemistry, University of Surrey, Guildford, United Kingdom.*

¶*Institut Laue-Langevin, 71 Avenue des Martyrs, CS 20156, F-38042 Grenoble Cedex 9, France.*

§*Instituto de Física Fundamental, Consejo Superior de Investigaciones Científicas, Serrano 123, E-28006 Madrid, Spain.*

E-mail: ic314@cam.ac.uk

Phone: +44 (0)1223 337279

Abstract

This work presents an experimental picture of molecular ballistic diffusion on a surface, a process which is difficult to pinpoint since it generally occurs at very short length scales. By combining neutron-time-of-flight data, with molecular dynamics simulations and density functional theory calculations, we provide a complete description of the ballistic translations and rotations of a poly-aromatic hydrocarbon (PAH) adsorbed on the basal plane of graphite. Pyrene, $C_{16}H_{10}$, adsorbed on graphite is a unique system where at relative surface coverages of about 10-20 %, its mean free path matches the experimentally accessible time/space scale of neutron time-of-flight spectroscopy (IN6 at the

Institut Laue-Langevin). The comparison between the diffusive behavior of large and small PAHs such as pyrene and benzene adsorbed on graphite, brings a strong experimental indication that the interaction between molecules is the dominating mechanism in the surface diffusion of poly-aromatic hydrocarbons adsorbed on graphite.

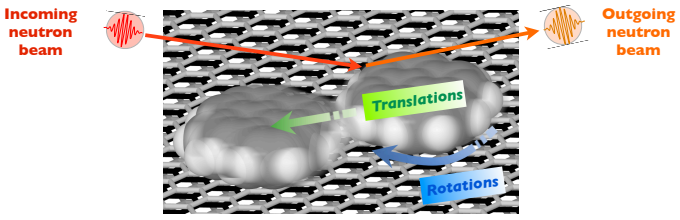

Carbon based materials play a central role in the search for low-friction building blocks in nanotechnology.[1–4] The high economical impact of wear, friction (energy dissipation) and lubrication in industry and transport[5] has fostered intensive research in friction free or super-diffusive systems.[6] Super-diffusivity has been observed in systems involving graphitic compounds: fullerenes,[7,8] metallic clusters[9] or graphene flakes adsorbed on graphite.[10,11] The existence of quadrupole or higher order interactions may cause the super-diffusivity between graphene and graphite observed with atomic force microscopy (AFM).[10,12,13] Interactions of the same nature exist in poly-aromatic hydrocarbons (PAH) adsorbed on graphitic substrates,[14,15] which are characterized by a very low energy barrier for lateral diffusion[16] and can act as nano-sized lubricants.[2]

Scattering techniques such as quasi-elastic helium atom scattering (QHAS) and quasi-elastic neutron scattering (QENS) are powerful tools to investigate very fast molecular dynamics (pico-second time scale and atomistic length scale).[17] Their combination provided the first unambiguous experimental observation of Brownian diffusion of molecules adsorbed on surfaces (benzene/graphite) as well as the first precise measurement of the kinetic friction parameter.[16,18] The sensitivity of QENS and QHAS to the dynamics of adsorbates on weakly corrugated surfaces (diffusion energy barrier in the meV range) turns them into the ideal probe for research into the origin of energy dissipation on graphite.[17,19,20]

At strong dilution, Brownian dynamics can transform into ballistic motion, i.e., molecular collisions where linear and angular momentum is exchanged, become negligible and molecules move in a linear fashion. Hints of ballistic dynamics were already found at very low relative coverages of benzene on graphite (0.1 monolayers (ML), corresponding to 10 % occupancy of the effective surface adsorption sites).[18] However, the observation of the pure ballistic regime requires an even lower density of adsorbates, which, in turn requires the use of molecules with a bigger size and a large scattering cross section to preserve an adequate signal-to-noise ratio. In the present work, we explore the diffusion of pyrene ($C_{16}H_{10}$) on graphite in the low coverage regime of 0.1 and 0.2 ML and for temperatures between 80 K and 350 K. We compare its diffusive behavior to benzene (C_6H_6) on graphite at equivalent relative coverages and temperatures. By combining the experimental data with density functional theory (DFT) calculations, molecular dynamics (MD) simulations and a new analytical model which predicts the signature of ballistic translations and rotations in QENS data, we achieve a full characterization of pyrene's diffusive behavior.

QENS measurements of 0.2 ML of pyrene and benzene at equivalent kinetic temperatures (where the ratio temperature to mass, T/m is the same) show how the molecular size allows to adjust the mean free path $\bar{l}$ for ballistic diffusion to the time and length scale covered by the neutron spectrometer. The values for the molecular radius and the mean free path expected for 0.2 ML of pyrene and benzene are summarized in Tab. 1. Accordingly, benzene's ballistic diffusion will be visible at momentum transfers of $Q_{ball} > 0.9$ Å^{-1}, while pyrene's ballistic diffusion is already visible at $Q_{ball} > 0.6$ Å^{-1}. Fig. 1 displays the distribution of neutron intensity, the so-called *scattering function* $S(Q, \Delta E)$ (SF),[21] as a function of the energy transfer ΔE, at a momentum transfer of $Q = 0.8$ Å^{-1} for 0.2 ML of benzene (at 60 K and 140 K) and 0.2 ML of pyrene (at 160 K and 320 K) respectively.

The molecule's diffusive behavior can be characterized qualitatively by analyzing the energy profile of the scattering function: A Gaussian form of the quasi-elastic spectrum is

Table 1: Summary of the relevant physical parameters for benzene and pyrene adsorbed on graphite for a relative coverage of $\theta = 0.2$ ML.

Physical Parameter	C_6H_6	$C_{16}H_{10}$
Area:[1] σ (Å^2)	37	~ 85
Molecule radius:[2] $a = \sqrt{\sigma/\pi}$ (Å)	3.5	5.2
Pair correlation:[3] $g(d_+)$	2.6	2.6*
Molecular density:[4] $\rho = \theta g(d_+)/(\sigma)$ (molecules.Å^{-2})	1.4×10^{-2}	0.6×10^{-2}
Mean free path: $\bar{l} = 1/(2\sqrt{2}\rho a)$ (Å)	7.2	10.9
Corresponding momentum transfer: $Q_{\rm ball} = 2\pi/\bar{l}$ (Å^{-1})	0.9	0.6
Energy for adsorption[5] (eV)	-0.64	-1.56
Energy barrier for diffusion[5] (eV)	0.012	0.011

[1] The value for the area occupied by a molecule lying flat on the basal plane of graphite σ (see Ref.[22] for benzene and DFT calculations for pyrene).
[2] The radius a of the adsorbed molecule.
[3] The pair correlation value at the first neighbour distance $g(d_+)$ (*we assume that benzene and pyrene have the same value, see Ref.[18]).
[4] The molecule density at the contact distance ρ
[5] The energy for adsorption and the barrier for diffusion have been calculated with DFT.

Table 2: Summary of the fit results of the benzene and pyrene experimental SFs at equivalent experimental conditions and for a relative coverage of $\theta = 0.2$ ML and a momentum transfer of $Q = 0.8$ Å^{-1}.

Physical Parameter	C_6H_6		$C_{16}H_{10}$	
Temperature (K)	60	140	160	320
Shape parameter: $\chi(Q = 0.8$ Å$^{-1})$	$0.3^{+0.5}_{-0.3}$	$0.3^{+0.5}_{-0.3}$	0.9 ± 0.4	1.0 ± 0.3
GoF[1] for Eq. 1	1.2	2.9	2.0	2.1
GoF for Lorentzian function fit	1.0	1.5	1.6	1.7
GoF for Gaussian function fit	2.6	2 .5	1.8	1.9

[1] Goodness of fit.

characteristic for ballistic diffusion. Conversely, a Lorentzian like profile of the energy transfer is the signature of Brownian diffusion.[20] In order to quantify the degree of ballistic/Brownian diffusion (Gaussian/Lorentzian like quasi-elastic profile) we fit the experimental SF to the convolution of the experimental resolution function (the vanadium scattering function) with a model function for diffusion on a flat potential energy surface:[23]

$$S_{inc}(Q,\Delta E) = y_0 + S_{res}(Q,\Delta E)\otimes \left[\exp[\chi^2(Q)] \times A(Q) \sum_{n=0}^{\infty} \frac{(-\chi^2(Q))^n}{\pi n!} \frac{(n+\chi^2(Q))\eta}{[(n+\chi^2(Q))\eta]^2 + \Delta E^2}\right]. \quad (1)$$

Here, y_0 is the background arising from processes which are too fast to be observed in the current time window (phonons for instance) and instrumental noise; $A(Q)$ is the global amplitude of the quasi-elastic signal, $\chi(Q) = \sqrt{\langle v^2\rangle}Q/\eta$ is the shape parameter, defined as the ration between the mean square velocity $\langle v^2\rangle$ and the friction parameter η.[23] Its value determines the energy dependence of the quasi-elastic profile:[23] i) for large η (Brownian diffusion) $\chi \ll 1$, and only the first term $n = 0$ of the summation in Eq. 1 contributes to the scattering function. ii) Conversely, if η is very small and $\chi \gg 1$, then Eq. 1 can be approximated by a Gaussian function which is the typical signature of ballistic diffusion.[20]

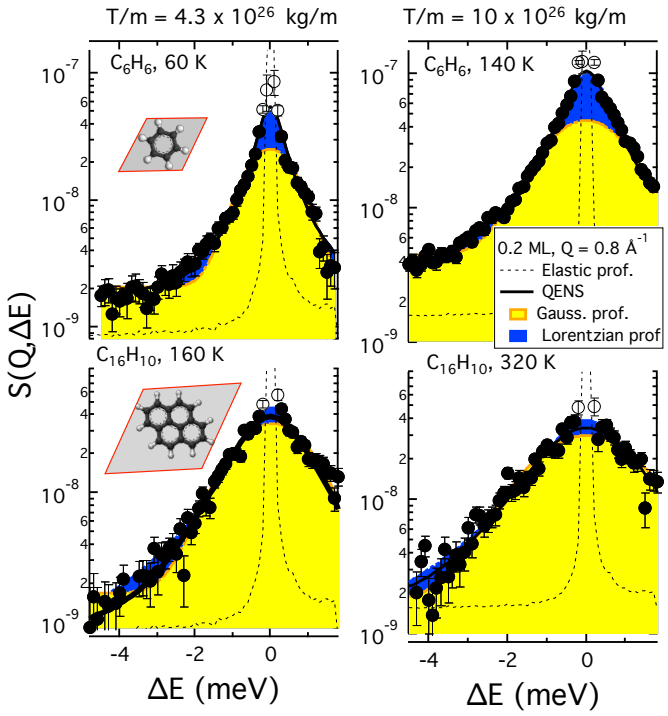

Figure 1: Comparison of the experimental scattering function $S(Q = 0.8\text{Å}^{-1}, \Delta E)$ for 0.2 ML of benzene at 60 K (top left) and 140 K (top right) and 0.2 ML of pyrene at 160 K (bottom left) and 320 K (bottom right). On the top of each graph we indicate the temperature/mass ratio: $4\times\ 10^{26}$ K.kg^{-}1 (left) and $10\times\ 10^{26}$ K.kg^{-}1 (right). The thick black line is the fitting of the experimental data to Eq. 1. The yellow area is the fit of the experimental data to a Gaussian function and the blue area is the fit of the experimental data to a Lorentzian function. The dotted black line is the elastic profile. The open circles mark the data points excluded from the GoF calculation.

Tab. 2 summarizes the result of the best fit while Fig. 1 shows the best fit for each experimental profile in comparison with a single Lorentzian and Gaussian function (further details can be found in the supplementary information). We observe that the fitted shape parameter χ for pyrene is equal to one while for benzene it is clearly below. Accordingly the benzene quasi-elastic profile is best fitted by a Lorenzian function and the pyrene quasi-elastic profile could be fitted with either a Gaussian or a Lorentzian function. Both options yield a very similar goodness of fit, GoF, in the range of energies which excludes the points within [-0.2,0.2] meV where the elastic signal dominates over the quasi-elastic signal. Therefore, benzene diffuses in a Brownian fashion (significant value of η) while pyrene displays hints

of ballistic diffusion at $Q = 0.8$ Å^{-1} ($\eta \ll 1$ and high degree of Gaussian-like quasi-elastic profile). In addition, the very low corrugation of the substrate potential energy surface calculated by DFT for both molecules, suggests that the role of the substrate in the friction dissipative process is small. The observation of a ballistic diffusive behavior in a dilute system (pyrene) and a Brownian diffusive regime in a denser system (benzene) supports the hypothesis that the origin of friction in PAH adsorbed on graphite is mostly due to collisions between molecules which act as rough hard disks and exchange linear and angular momentum.[18] The main channel for the translational kinetic energy dissipation is therefore the conversion of linear motion into rotations and other internal degrees of freedoms: tumbling for benzene and internal vibrations for pyrene (see the last section of supplementary information). In the following paragraph we attempt to fully characterize pyrene's diffusive behavior.

Fig. 2 displays the quasi-elastic neutron spectra measured in pyrene/graphite samples at two different relative coverages: 0.1 ML and 0.2 ML, at 320 K, and calculated from molecular dynamics simulations of a full molecule and its center of mass (C.o.M) trajectories. The energy profiles are fitted to a model which combines an elastic peak (in the case of experimental data), a quasi-elastic peak arising from ballistic translations and rotations and an inelastic contribution whose origin we have explored with DFT calculations (see supplementary information):[1]

$$S_{fit}(\mathbf{Q},\Delta E) = y_0 + \left[A_{el}(Q)\delta(\Delta E)A(Q) + A(Q)S_{BTR}(\mathbf{Q},\Delta E) + \frac{A_p(Q)}{(\Delta E - \Delta E_p(Q))^2 + \Gamma_p(Q)^2} \right] \quad (2)$$

The free parameters in the fitting are the flat background y_0, the elastic peak amplitude $A_{el}(Q)$ (in the case of the experimental data), the global amplitude of the quasi-elastic profile $A(Q)$, the energy $\Delta E_p(Q)$, the amplitude $A_p(Q)$ and the width $\Gamma_p(Q)$ of the inelastic

[1]Note that for the experimental data, Eq. 2 needs to be convoluted with the resolution function (the vanadium scattering function): $S_{res}(\mathbf{Q},\Delta E) \otimes S_{fit}(\mathbf{Q},\Delta E)$

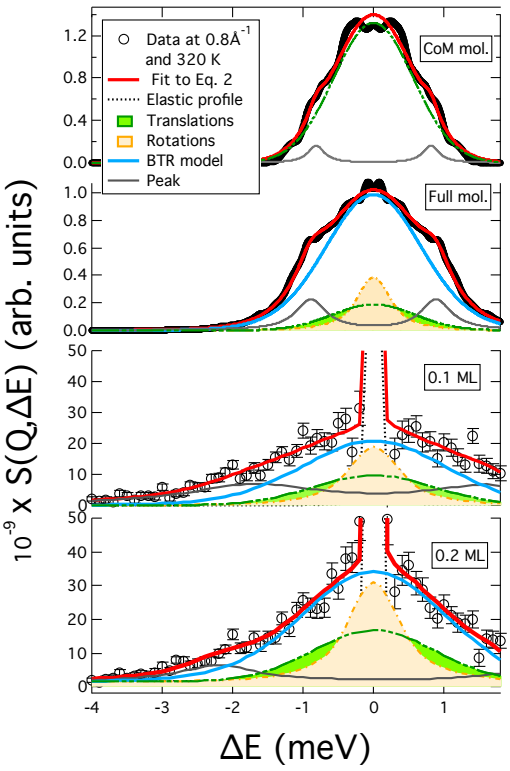

Figure 2: Simulated and experimental scattering functions (SF) at a momentum transfer of 0.8 Å^{-1} and at 320 K. *1st and 2nd panel*: Simulated SFs extracted from the center of mass (CoM) and the full molecule trajectories in the MD simulation, respectively. *3rd and 4th panel*: Experimental SFs of 0.1 ML and 0.2 ML of pyrene/graphite.

peak. $S_{BTR}(\mathbf{Q},\Delta E)$ stands for the *ballistic translational rotational (BTR)* model consisting in the convolution of a classical Gaussian function, typical for ballistic translations, with an adaptation of the scattering function for uniaxial rotational diffusion[24] to the ballistic regime (see Eq. 14 in the supplementary information):

$$\begin{aligned} S_{BTR}(\mathbf{Q},\Delta E) &= S_T(\mathbf{Q},\Delta E) \otimes S_R(\mathbf{Q},\Delta E) \\ &= \sum_{k=1}^{N_H} \left[J_0^2(Qa_k) S_T(Q,\Delta E) + 2\sum_{l=1}^{\infty} J_l^2(Qa_k) S_T(Q,\Delta E) \otimes S_R(l,\Delta E) \right] \end{aligned} \tag{3}$$

The ballistic rotational scattering function is a summation of Gaussian profiles $S_R(l,\Delta E)$, whose half-width-at-half-maximum (HWHM) is determined by the angular mean square velocity (in analogy to the translational case) but is independent of the momentum transfer

(due to confinement[24,25]). Each term of the sum is weighted by the cylindrical Bessel function $J_l(Qa_k)$ of the l-th order which takes into account the geometry of the motion. a_k is the radius of the circle on which each scatterer moves when the molecule rotates. In the case of hydrogenated pyrene, $C_{16}H_{10}$, the scattering intensity is dominated by the incoherent scattering cross section of the protons, and therefore k accounts only for the N_H hydrogen atoms in the molecule.[20]

The fit of the experimental data to the model (Eq. 3) yields an excellent agreement, for the values of $\langle v^2 \rangle$ and $\langle \omega^2 \rangle$ predicted by the equipartition theorem for 2D translations and uniaxial rotation: 2.69 $\text{Å}^2.\text{ps}^{-2}$ and 0.18 ps^{-2}, respectively. The translational and rotational quasi-elastic profiles have a distinct HWHM due to their different time scale: $\sim$15 ps for a 2π rotation of the molecule versus $\sim$ 5 ps for a distance of 8 Å (corresponding to $Q \sim 0.8$ Å^{-1}). The MD simulations show a similar behavior where translations and rotations also display separable time scales. The values obtained for $\langle v^2 \rangle$ and $\langle \omega^2 \rangle$, 1.26 $\pm$ 0.02 $\text{Å}^2.\text{ps}^{-2}$ and 0.075 $\pm$ 0.001 ps^{-2} respectively, are smaller than the predictions of the equipartition theorem, but their ratio of 16.8 is in accordance with the theoretical ratio of 13.6, which is determined by the ratio between the mass and the moment of inertia of pyrene. Therefore, we obtain qualitatively the same behavior of the quasi-elastic profile for simulated and experimental data.

The signature of the molecular diffusive regime can also be found in the *quasi-elastic broadening* Γ,[20] taken as the HWHM of the quasi-elastic profile. Fig. 3 shows the quasi-elastic broadenings extracted from the fit of 0.1 ML, 0.2 ML and simulations to Eq. 2 as a function of coverage, the momentum transfer (panels A and B) and temperature (panel C)[2]. It also compares them with the predictions of the BTR model. Panel D shows a scheme of the translational-rotational dynamics of the molecules generated from the MD simulated trajectories.[26]

[2]The error in the quasi-elastic broadening is calculated by evaluating Eq. 2 in the limits of the confidence band of the fitted parameters. The resulting error bar is of the size of the symbol.

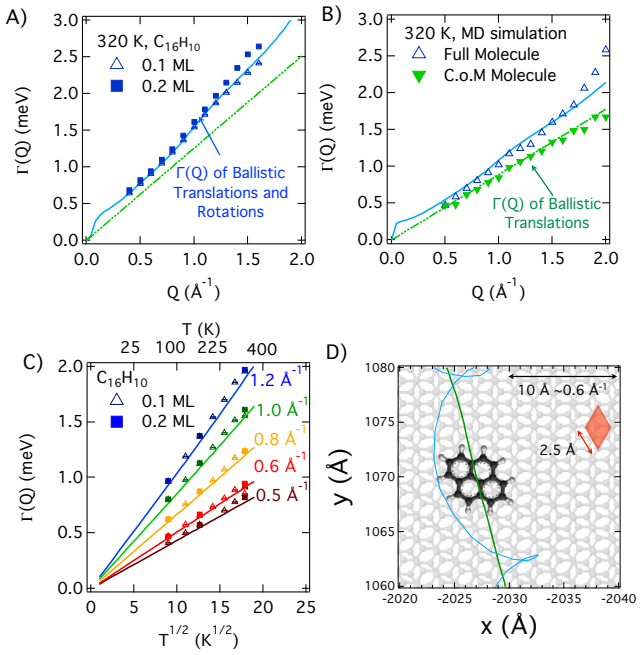

Figure 3: *Panel A*: Quasi-elastic broadening versus the momentum transfer, extracted from the fitted profile of the experimental data to Eq. 2. *Panel B*: Quasi-elastic broadenings extracted from the fit to Eq. 2 of the simulated SF. *Panel C*: The experimental quasi-elastic broadening for 0.1 and 0.2 ML versus the temperature. In all the three panels, the solid lines are the prediction for the quasi-elastic broadening of the BTR model. *Panel D*: Schematic representation of the dynamics of the molecule as observed in the MD simulation:[26] with a green line we represent the center of mass motion and with a blue line, the trajectory of one of the protons of the molecule. The red area represents the graphite unit cell.

We observe the following: i) the quasi-elastic broadening is independent of coverage, in all the momentum transfer range (panel A), and also in a very wide thermal range (panel C). ii) Panel A shows how rotations deviate the quasi-elastic broadening dependence on Q from the linear law. iii) Panel C confirms that the quasi-elastic broadening is proportional to $\sqrt{T}$. Thus, we conclude that the main part of the quasi-elastic intensity comes from the ballistic translations and rotations of the pyrene molecules on the surface and is well reproduced by the BTR model. The panel B displays the quasi-elastic broadenings extracted from the fit of the MD simulated scattering functions to Eq. 2. Qualitatively, the MD simulations deliver a picture of the diffusive behavior of a single pyrene molecule matching the experimental observations. The center of mass (C.o.M) of the molecule follows a linear law of the momen-

tum transfer, as expected for ballistic translations, while the total quasi-elastic broadening (calculated from the trajectories of the full molecule) deviates from the linear law of Q and follows the BTR model. Note, that for the MD simulations the agreement with the model is achieved by considering either an effective mass and an effective momentum of inertia which are larger than the real values of the pyrene molecule, or an effective temperature which is below 320 K.

Finally, we consider several possibilities for the origin of the inelastic feature in the quasi-elastic spectrum of pyrene. The inelastic feature may be caused by the low energy phonons of graphite along the [0001] direction,[27] which we are observing due to the misalignment of graphite crystallites in the Papyex substrate.[28] We have also explored the effect of molecular tumbling (librations around the x or y axis resulting into a motion along the z axis). DFT calculations provide a potential well for the tilting of pyrene with respect to the substrate plane (see the supplementary information). From the quadratic part of the well, we estimate the frequency of an oscillatory motion along the z axis whose ground energy is $\Delta E = \hbar\omega/2 = 0.4$ meV. Another possibility are external vibrations of the whole molecule with respect to the surface, which can also give rise to vibrations within this energy range as observed on metal substrates.[29]

In summary, we have studied the diffusive behavior of pyrene adsorbed on exfoliated graphite using quasi-elastic neutron scattering over a large thermal range (80 K up to 320 K) and for a coverage of 0.1 ML and 0.2 ML. The dependency of the quasi-elastic signal on energy transfer momentum transfer, coverage and temperature, suggests that pyrene diffuses ballistically on the basal plane of graphite. The comparison with the Brownian diffusion observed for benzene under equivalent experimental conditions, brings a strong support for the description of friction processes in PAH/graphite systems as the result of molecular collisions: we observe how surface friction vanishes at strong dilution.

To fully characterize the ballistic diffusive regime of the pyrene molecule on the basal

plane of graphite, we have developed a new model (BTR) to identify the experimental signature of friction free-translations and rotations. DFT calculations complement the interpretation of the experimental data by providing a very low energy barrier for diffusion of 11 meV and a potential well for the tumbling of the molecule on the substrate. Finally MD simulations of a single pyrene molecule on graphite reproduce qualitatively the experimental observations and allow to separate the purely translational part from the rotational part of the scattering function.

Thus the study of PAH on graphitic surfaces represents a wide territory for the investigation of different diffusive motions. The present work leaves several open questions which we hope will encourage further studies of the surface dynamics of weakly physisorbed systems: The role of tumbling in the friction dissipation process of PAH's kinetic energy is still an open issue. Moreover, measurements of even larger PAH such as coronene could provide a deep insight into the role of size and rotations in the diffusion of PAH on graphite.

1 Experimental procedure

The measurements were performed at the IN6 time-of-flight spectrometer of the ILL. The incoming neutron wavelengths was set to 5.12 Å with an energy resolutions at full width, half maximum of 70 μeV. The neutron scattering signal of the adsorbate molecules was enhanced by using Papyex exfoliated graphite substrates (grade N998, $>$ 99.8 % C, Carbone Lorraine), which have a high specific surface area of the order of 23 m^2g^{-1} [28] and a preferential orientation of the graphite crystallites with their basal plane parallel to the scattering plane (in–plane scattering geometry).[28,30] In addition, the coherent length of the crystallites extracted from the x-ray diffraction pattern is, on average, 600 Å.[28] Hence, we expect the impact of edges and defects to be negligible for the diffusion process, given that the pyrene mean free path is of 10 Å. The specific surface area of the samples was verified by the

Brunauer-Emmett-Teller (BET) nitrogen adsorption isotherms. We used liquid He cryostats as sample environment to control the temperature within the range of 1.7-320 K. We have performed measurements of 0.1 and 0.2 ML pyrene in the thermal range of 80 K to 320 K and of 0.2 ML of benzene at 60 K and 140 K. In addition, we have measured also the scattering function of the clean graphite substrate (before adsorption) as reference for substrate contributions and the resolution function of the instrument was measured using a sample of vanadium with the same geometry as the actual sample.

Acknowledgement

I. Calvo-Almazán is grateful to the Ramón Areces foundation for the funding of her post-doctoral research position. She is also very grateful to Dr. W. Allison, Dr. N. Avidor and Dr. M. A. Gonzalez for many helpful discussions. M. Sacchi thanks the UK's HEC Materials Chemistry Consortium, which is funded by EPSRC (EP/L000202), this work used the ARCHER UK National Supercomputing Service. E. Bahn acknowledges financial support by the graduate college of the Université de Grenoble (France) and A. Tamtögl would like to thank the FWF (Austrian Science Fund) for financial support within the project J3479-N20. S. Miret-Artés acknowledges the funding from the project FIS2014-52172-C2-1-P, from Ministerio de Economia y Competitividad (Spain). The authors acknowledge the generous provision of neutron beam time at ILL, the support by technicians and the CS laboratory where the MD simulations have been carried out.

Supporting Information Available

Details on the sample preparation, the molecular dynamics (MD) simulations, the density functional theory (DFT) calculations; description of the ballistic translational-rotational analytical model, the fit of the experimental data and the MD simulated trajectories; results

of the DFT calculations.

References

(1) Barreiro, A.; Rurali, R.; Hernández, E. R.; Moser, J.; Pichler, T.; Forró, L.; Bachtold, A. Subnanometer Motion of Cargoes Driven by Thermal Gradients Along Carbon Nanotubes. *Science* **2008**, *320*, 775–778.

(2) Scharf, T.; Prasad, S. Solid Lubricants: a Review. *J. Mater. Sci.* **2013**, *48*, 511–531.

(3) Krim, J. Friction and Energy Dissipation Mechanisms in Adsorbed Molecules and Molecularly Thin Films. *Adv. Phys.* **2012**, *61*, 155–323.

(4) Browne, W. R.; Feringa, B. L. Making Molecular Machines Work. *Nat. Nanotechnol.* **2006**, *1*, 25–35.

(5) Persson, B. N. J. *Sliding Friction. Physical Principles and Applications*, 2nd ed.; Springer: Berlin, 2000.

(6) Zheng, Q.; Liu, Z. Experimental Advances in Superlubricity. *Friction* **2014**, *2*, 182–192.

(7) Legoas, S. B.; Giro, R.; Galvão, D. S. Molecular Dynamics Simulations of C60 Nanobearings. *Chem. Phys. Lett.* **2004**, *386*, 425 – 429.

(8) Miura, K.; Kamiya, S.; Sasaki, N. C-60 Molecular Bearings. *Phys. Rev. Lett.* **2003**, *90*, 055509–4.

(9) Guerra, R.; Tartaglino, U.; Vanossi, A.; Tosatti, E. Ballistic Nanofriction. *Nature Mat.* **2010**, *9*, 634 – 637.

(10) Dienwiebel, M.; Verhoeven, G. S.; Pradeep, N.; Frenken, J. W. M.; Heimberg, J. A.; Zandbergen, H. W. Superlubricity of Graphite. *Phys. Rev. Lett.* **2004**, *92*, 126101–4.

(11) Lebedeva, I. V.; Knizhnik, A. A.; Popov, A. M.; Ershova, O. V.; Lozovik, Y. E.; Potapkin, B. V. Diffusion and Drift of Graphene Flake on Graphite Surface. *J. Chem. Phys.* **2011**, *134*, 104505–14.

(12) Verhoeven, G. S.; Dienwiebel, M.; Frenken, J. W. M. Model Calculations of Superlubricity of Graphite. *Phys. Rev. B* **2004**, *70*, 165418–10.

(13) Yang, J.; Liu, Z.; Grey, F.; Xu, Z.; Li, X.; Liu, Y.; Urbakh, M.; Cheng, Y.; Zheng, Q. Observation of High-Speed Microscale Superlubricity in Graphite. *Phys. Rev. Lett.* **2013**, *110*, 255504–5.

(14) Vernov, A.; Steele, W. A. Computer Simulations of Benzene Adsorbed on Graphite. 1. 85 K. *Langmuir* **1991**, *7*, 3110–3117.

(15) Vernov, A.; Steele, W. A. Computer Simulations of Benzene Adsorbed on Graphite. 2. 298 K. *Langmuir* **1991**, *7*, 2817–2820.

(16) Hedgeland, H.; Fouquet, P.; Jardine, A. P.; Alexandrowicz, G.; Allison, W.; Ellis, J. Measurement of Single Molecule Frictional Dissipation in a Prototypical Nanoscale System. *Nature Phys.* **2009**, *5*, 561–564.

(17) Jardine, A. P.; Hedgeland, H.; Alexandrowicz, G.; Allison, W.; Ellis, J. Helium-3 Spin-Echo: Principles and Application to Dynamics at Surfaces. *Prog. Surf. Sci.* **2009**, *84*, 323–379.

(18) Calvo-Almazán, I.; Bahn, E.; Koza, M.; Zbiri, M.; Maccarini, M.; Telling, M.; Miret-Artés, S.; Fouquet, P. Benzene Diffusion on Graphite Described by a Rough Hard Disk Model. *Carbon* **2014**, *79*, 183 – 191.

(19) Alexandrowicz, G.; Jardine, A.; Fouquet, P.; Dworski, S.; Allison, W.; Ellis, J. Observation of Microscopic CO Dynamics on Cu(001) Using He-3 Spin-Echo Spectroscopy. *Phys. Rev. Lett.* **2004**, *93*, 156103–4.

(20) Bée, M. *Quasielastic Neutron Scattering*; Adam Hilger: Bristol, 1988.

(21) Fouquet, P.; Calvo-Almazán, I.; Koza, M.; Tamtögl, A.; (2015), Diffusion of Pyrene Molecules: the Transition to Ballistic Diffusion. Institut Laue-Langevin (ILL). doi:10.5291/ILL-DATA.7-05-440.

(22) Bardi, U.; Magnanelli, S.; Rovida, G. LEED Study of Benzene and Naphthalene Monolayers Adsorbed on the Basal Plane of Graphite. *Langmuir* **1987**, *3*, 159–163.

(23) Martínez-Casado, R.; Vega, J. L.; Sanz, A. S.; Miret-Artes, S. Quasi-Elastic Peak Lineshapes in Adsorbate Diffusion on Nearly Flat Lurfaces at Low Coverages: the Motional Narrowing Effect in Xe on Pt(111). *J. Phys.: Condens. Matter* **2007**, *19*, 176006.

(24) Dianoux, A. J.; Volino, F.; Hervet, H. Incoherent Scattering Law for Neutron Quasi-Elastic Scattering in Liquid Crystals. *Mol. Phys.* **1975**, *30*, 1181–1194.

(25) Volino, F.; Dianoux, A. Neutron Incoherent Scattering Law for Diffusion in a Potential of Spherical Symmetry: General Formalism and Application to Diffusion Inside a Sphere. *Mol. Phys.* **1980**, *41*, 271–279.

(26) Jmol: an open-source Java viewer for chemical structures in 3D. `http://www.jmol.org/`.

(27) Wirtz, L.; Rubio, A. The Phonon Dispersion of Graphite Revisited. *Sol. State Comm.* **2004**, *131*, 141–152.

(28) Gilbert, E. P.; Reynolds, P. A.; White, J. W. Characterisation of a Basal-Plane-Oriented Graphite. *J. Chem. Soc., Faraday Trans.* **1998**, 1861–1868.

(29) Witte, G. Low Frequency Vibrational Modes of Adsorbates. *Surf. Sci.* **2002**, *502–503*, 405 – 416.

(30) Bockel, C.; Coulomb, J.; Dupont-Pavlovsky, N. Comparison of the Adsorptive Properties of Papyex and Uncompressed Exfoliated Graphite. *Surf. Sci.* **1982**, *116*, 369 – 379.